Chapter 4

4. Numerical Simulation of the Strain-Softening Behaviour

4.1 General

This chapter describes the approach to simulate the strain-softening behaviour of coal for varying width-to-height ratios. This approach considered the effect of the shear strength of contact surfaces at the ends of the specimen (interface effect), dilatancy, and zone size on the post-failure behaviour of the coal material. Based on the hit-and-trial technique, the numerical modelling-based experimentation was carried out to calibrate the stress-strain curves against the laboratory observed curves for width to height ratio varying from 0.5 to 13.5 for six different Indian coal seams as reported by Das (1986). A set of statistical models were developed using the post-peak softening parameters of 126 calibrated models to determine the post-peak softening parameters of coal. The validity of these models was also established by comparing the numerical modelling results with the triaxial test results reported by Medhurst (1996) for coal samples of different sizes.

4.2 Constitutive Behaviour

Laboratory testing, field measurements and numerical modelling have shown that the strength of the rocks reduces with deformation (Wawersik and Fairhurst, 1970; Das, 1986; Jaiswal and Shrivastava, 2009; Zhao and Cai, 2010; Prassetyo, 2011). This strain-softening behaviour is mainly attributed due to crack initiation, crack propagation and crack correlation. During the process of strain-softening, either pre-existing cracks are enlarged, or some new cracks are formed, leading to an increase in rock volume. The increase of rock volume due to inelastic deformation is known as dilation. These phenomena are modelled using a failure criterion and

non-associated plastic flow rule in continuum mechanics. The damage in the rock is quantified in terms of plastic shear strain. The peak strength of the rock is fixed by assigning suitable values to the strength parameters according to the failure criterion. The dilation behaviour of rock is represented using the dilation angle, represented by the slope of the volumetric strain vs the axial strain curve. The strain-softening nature is simulated through shrinkage of the failure criterion, which is achieved by mobilising strength parameters as the plastic deformation evolves.

Mohr-Coulomb and Hoek-Brown are the two well-known failure criteria for the rocks. However, the former is derived using the basic concepts of mechanics where strength parameters have physical meaning, and the latter is empirically derived where its parameters are determined from curve fitting. In this thesis, the Mohr-Coulomb criterion is used as it has a physical explanation. The cohesion and friction in the Mohr-Coulomb strength parameters are 'inherent cohesion' and 'internal friction' between the rock grains.

Previous researchers have adopted three approaches to simulate softening phenomena using the Mohr-Coulomb failure criterion (Please refer to Section 2.6.2, Chapter 2). In all these approaches, the cohesion is degraded to its residual value as plastic deformation evolves in the rocks. However, these approaches have different takes on the friction angle of rocks in the post-failure regime. In the first approach, the friction angle is mobilised after the cohesion begins to degrade. Hence, a very low friction angle is initially assigned to the material, increasing to its maximum value as the plastic strain increases (Hajiabdolmajid et al., 2002; Diederichs, 2007; Edelbro, 2009; Walton, 2019). This approach is based on the theory that the frictional component of strength is active when there is a movement against the surface, which happens only after the crack formation leading to loss of cohesive strength.

The second approach advocates that the internal friction angle depends on the surface conditions, which remain largely unaltered during the damage process (Pourhosseini and

Shabanimashcool, 2014; Jiang et al., 2017; Le et al., 2018). Hence, the friction angle remains constant. In the third approach, friction is decreased along with cohesion as plastic damage evolves to model the strain-softening characteristics of rocks (Mohan et al., 2001; Feng et al., 2019; Wang et al., 2015; Bai et al., 2017). The decrease in friction angle can be attributed to shearing off of asperities along the shear plane. The asperities at the freshly exposed surfaces due to crack propagation and correlation reduce because of the movement against each other as the axial deformation advances. The effective friction angle of the surface is the summation of the basic friction angle of the rock and the roughness angle (Figure 4.1) (Wyllie and Norrish, 1996). This effective friction angle reduces due to shearing off of asperities with the displacement along the surface. Consequently, the friction angle is the function of the normal stress, compressive strength of the rock, and displacement along the surface. Hence, friction angle should reduce with the advance of deformation at the strain-softening stage.

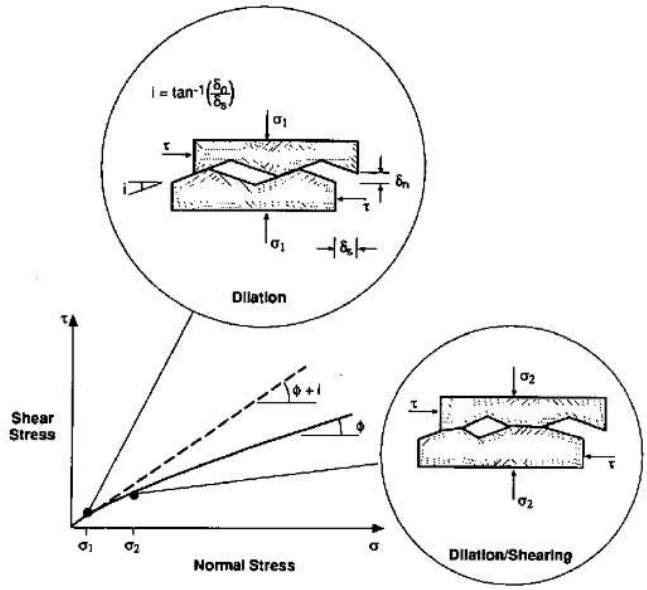

Figure 4.1 Effective friction angle of the surface due to surface roughness and normal stress (after Wyllie, 1992)

4.3 Post-Peak Strength Parameters

A numerical modelling study was conducted to establish the approach for estimating the post-peak strength parameters of the MCSS constitutive model. The study involved modelling the stress-strain behaviour of coal samples of different w/h ratios for the entire range of their loading up to the residual strength for six Indian coal seams belonging to Raniganj, Jharia, and South Karanpura coalfields, as reported by Das (1986).

The details of the laboratory tests conducted by Das (1986) are presented in Section 2.6.2, Chapter 2. The laboratory tests showed that the samples regained strength for w/h $\geq$ 4-6 after initially decreasing for a small segment of post-failure strain. The post-peak strength of the samples with a lesser w/h ratio dropped to zero, signifying brittle failure with no residual strength. The test showed perfectly ductile behaviour for w/h $\geq$10 and a strain-hardening nature beyond this.

The post-peak parameters were determined in two steps. In the first step, the initial range of the variation of post-peak strength parameters was fixed based on the previous studies. Later, the hit-and-trial technique was used to calibrate the model observed stress-strain curves against the laboratory observed profile and finalise the parameters. The grid generation method, model geometry, and boundary conditions have been discussed in Section 3.10, Chapter 3.

Das (1986), Das and Sheorey (1986), and Sheorey et al. (1986) reported the laboratory test results (Figure 4.2) of coal samples obtained from six Indian coal seams. The uniaxial compressive strength (UCS) and elastic modulus (E) were determined from the uniaxial compression testing of the coals, whereas the friction angle was evaluated from the servo-controlled triaxial testing using Hoek and Franklin cell. The cohesion was estimated from the UCS and friction angle, assuming that coal behaves as the Mohr-Coulomb material. Rashed and Peng (2015) conducted direct shear tests using GCTS Rock Direct Shear System RDS-200

to determine the shear strength of contact surfaces between the coal specimen ends and the machine platens. The test results showed that the internal friction angle of the contact surfaces was approximately 14°.

Table 4.1 shows the interface stiffness parameters as per the approach suggested in the manual (Section 3.4, Chapter 3). The W-D dilation angle model parameters, as already defined in Section 3.5.2, Chapter 3, are mentioned in Table 4.2.

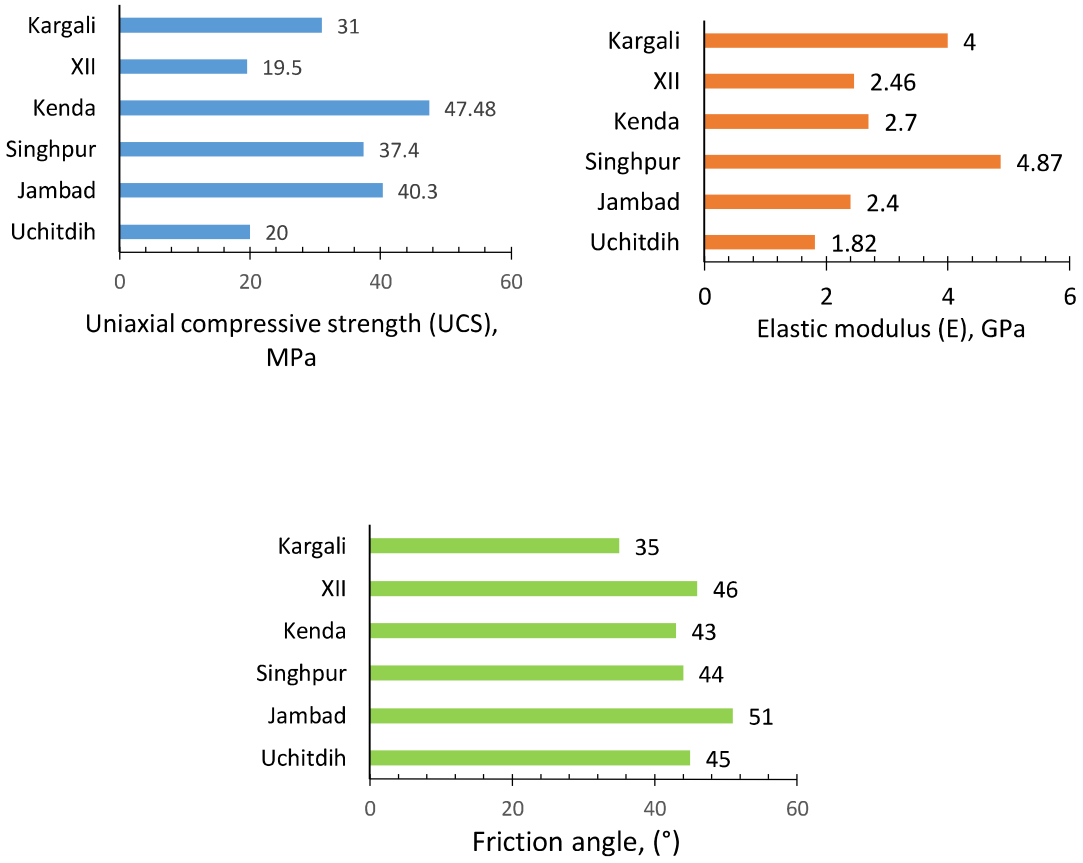

Figure 4.2 Charts depicting the input properties of coal in the model

Table 4.1 Interface properties considered in the model

Normal and Shear stiffnesses, GPa/m (Equation 3.2)	Friction angle, (°)	Cohesion, Pa	Dilation, (°)
$\mathbf{10 \cdot max}\left[\frac{\left(K+\frac{4}{3}G\right)}{\Delta z_{min}}\right]$	14	1000	7

Table 4.2 Input parameters of the W-D dilation angle model used in the numerical modelling (after Walton and Diederichs, 2015)

α_0	α'	γ_m(mstrain)	γ_0 (mstrain)	γ' (mstrain)
0.17	0.045	0.001	0.12	0.025

4.4 Drop Rates and Residual Cohesion and Friction angle

In this study, cohesive strength and friction angle were reduced to their residual values during the strain-softening regime. Figure 4.3 shows the schematic diagram for a typical strain-softening implementation in the Mohr-Coulomb model. In the FLAC^{3D} implementation, a piecewise-linear softening law for the strength parameters was prescribed as a function of plastic shear strain. In addition to the elastic parameters, the MCSS model requires six parameters: $\boldsymbol{c_{peak}}$, $\boldsymbol{c_{res}}$, $\boldsymbol{\phi_{peak}}$, $\boldsymbol{\phi_{res}}$, $\boldsymbol{e_c^{ps}}$ and $\boldsymbol{e_\phi^{ps}}$ along with mobilisation of dilation angle ($\boldsymbol{\psi}$) as a function of evolving plastic shear strain ($\boldsymbol{e^{ps}}$). For the sake of convenience, cohesion ($\boldsymbol{c_{Drop}}$) and friction angle ($\boldsymbol{\phi_{Drop}}$) drop rates were introduced to replace $\boldsymbol{e_c^{ps}}$ and $\boldsymbol{e_\phi^{ps}}$, respectively, while performing iterative modelling using the trial-and-error technique. Here, post-peak softening of the strength parameters is assumed to follow the bilinear-decay profile.

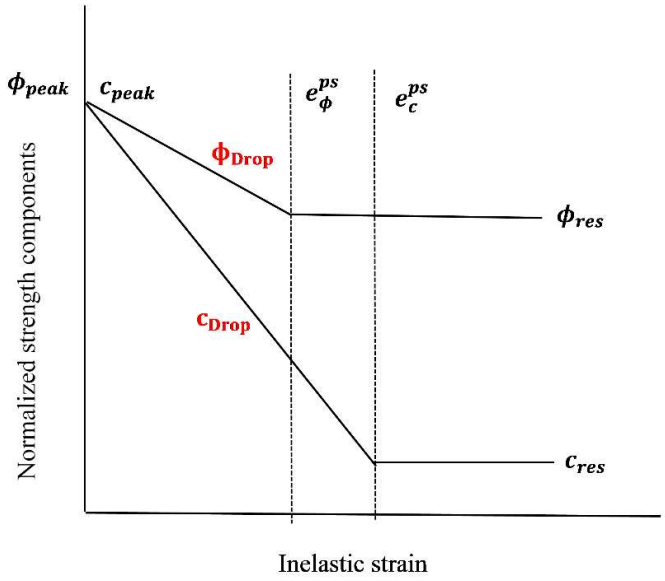

Figure 4.3 Schematic illustrating the evolution of strength components, friction angle and cohesion as a function of inelastic strain in the MCSS constitutive model

Several researchers (Zhao et al., 2014; Zhang et al., 2018; Feng et al., 2019; Jiang et al., 2017; Li et al., 2015; Bai et al., 2014; Bai et al., 2017; Wang et al., 2015; Shabanimashcool and Li, 2012; Mohan et al., 2001; Yan et al., 2013) have used the MCSS model to design and evaluate the stability of mining structures. A wide range of post-peak parameters was used in these studies (Section 2.6.2, Chapter 2) based on the back-analyses of failure patterns, stress-strain curves, displacement, and stress in the coal pillars and samples. The cohesion drop varied from 16 to 423 MPa, while the friction drop rate varied from 400° - 1200° per unit of plastic shear strain. The residual cohesion and friction angle range from 0 to 35% and 71 to 88% of their peak values, respectively. The median values of the cohesion and friction drop rates are 161 MPa and 700° per unit of plastic shear strain, and their residual values are 10% and 79% of the peak values, respectively.

Different drop rates and residual values were attempted to calibrate the model observed stress-strain curve for a given zone size and w/h ratio of the sample against the laboratory-observed

characteristics of the sample of similar w/h ratio. The initial range of variation in these parameters was based on the data compiled from the literature. Figure 4.4 shows the scheme of iterative techniques adopted for the calibration based on hit-and-trial for a given zone size of the model.

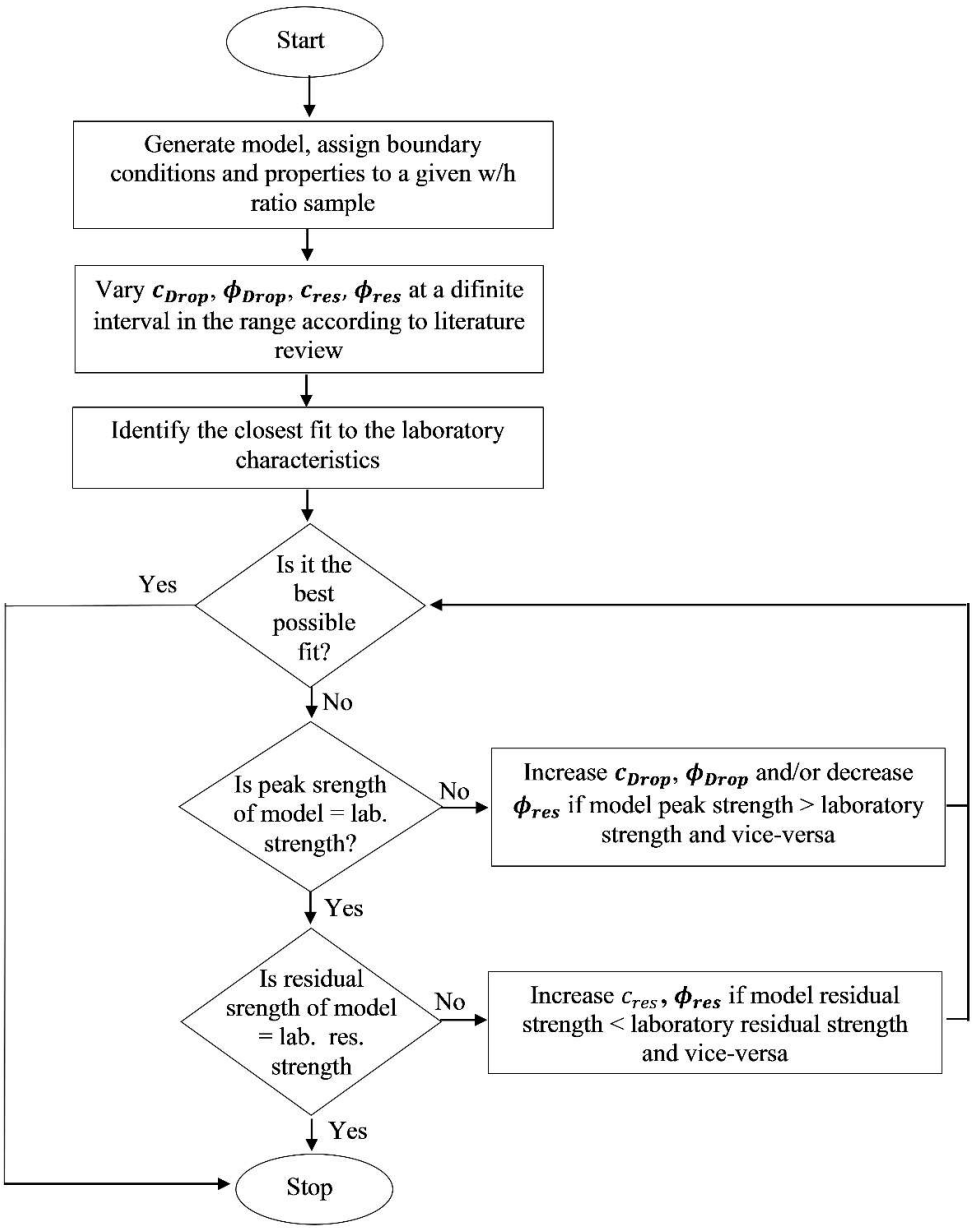

Figure 4.4 The scheme of the iterative technique used to calibrate the model stress-strain curve against the laboratory curve for a give w/h ratio sample based on hit-and-trial

Table AIII.1 (Annexure-III) summarises the final drop rates and residual values of cohesion and friction angle of 126 calibrated models for samples of various w/h ratios from six different Indian coal seams for zone sizes of 0.5, 1, and 2 mm. The model observations showed that while all the four parameters have a considerable effect, cohesion drop rate and residual value have a more significant influence on the mechanical behaviour of the modelled coal sample. The peak strength was reduced with an increase in cohesion and friction drop rates, as well as the residual value of the friction angle. On the other hand, residual strength was increased with the increase in the residual cohesion and friction angle. The residual strength was found to be primarily a function of residual cohesion. The zone size significantly affected the peak and post-peak strengths of the modelled sample. With the increase in zone size, the peak and residual strengths increased.

The observations from the calibrated models show that the samples from a given coal seam have different post-peak strength parameters depending upon the w/h ratio. The friction angle drop rate of 100, 300, and 500°/plastic shear strain and the residual value of 50 and 70% of the peak value were sufficient to calibrate the model for different strength properties and elastic modulus for w/h ratio ranging from 0.5-13.5. The cohesion drop rate increased with the w/h ratio and the zone size. The residual cohesion varied from 0-20% of the peak value and was zero for w/h $\leq$ 2.

Figure 4.5 compares the modelled stress-strain characteristics with their laboratory observed trend for samples of the Singhpur middle coal seam. The modelling results are in close agreement with the laboratory observation. The peak and the residual strengths of the modelled samples increased with the w/h ratio, whereas the post-peak stiffness decreased with an increase in the w/h ratio. The model with a w/h ratio of 0.5 and 1.0 showed perfectly brittle behaviour and had a very high drop rate, whereas the model with a w/h of 7.7 exhibited perfectly plastic behaviour and had a nominal drop rate. The models having w/h of 2, 3, and

4.5 showed strain-softening behaviour through a gradual loss of strength from their peak to the residual values. The models for w/h greater than 7.7 showed strain-hardening characteristics.

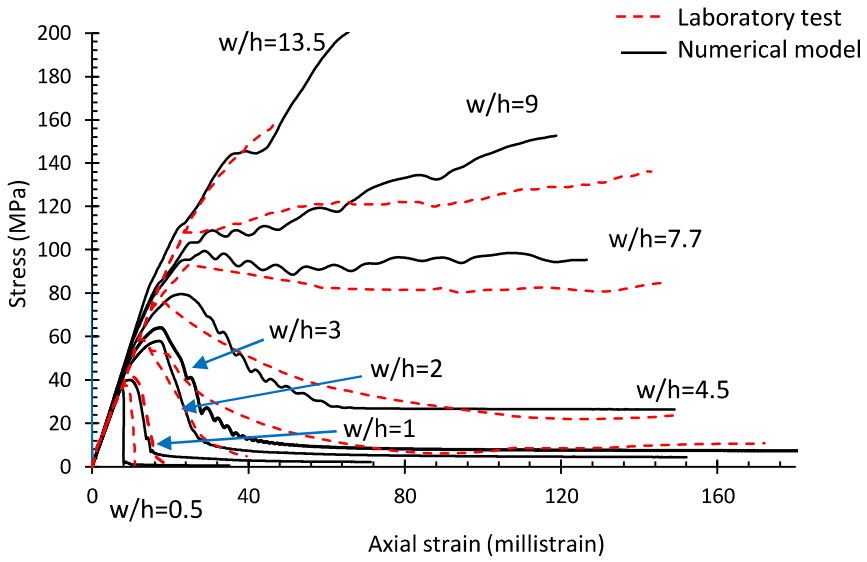

Figure 4.5 Comparison between the model observed and the laboratory test results of the coal samples of varying w/h ratio from the Singhpur middle seam

Dilation is the fundamental and pervasive volumetric property of the rocks (Cook, 1970). Dilatancy and post-peak parameters of the MCSS model are closely related as both determine the evolution of plastic shear strain. Figure 4.6 shows the model observed volumetric vs axial strain characteristics for various w/h ratios of Singhpur middle coal samples. The volumetric strain starts to decrease with the axial strain till the point of reversal, which corresponds to the pre-peak portion of the stress-strain curve (Figure 4.5), where the already existing pores and micro-cracks get compacted. Beyond this point, the existing cracks begin to propagate, and new cracks are formed with the continuance of further axial strain. The point of reversal corresponds to the state where the density of cracks is sufficient to merge and develop shear bands or tensile spalls. With a further increase in loading, the dilation begins to increase

substantially. With the continuation of loading, the dilation does not grow at the same rate but decreases and becomes constant. The points where the curves cross the axial strain axis represent the state at which the volumetric compaction due to the closure of the existing pores and cracks is equal to the volumetric expansion caused by the formation of new cracks with further loading.

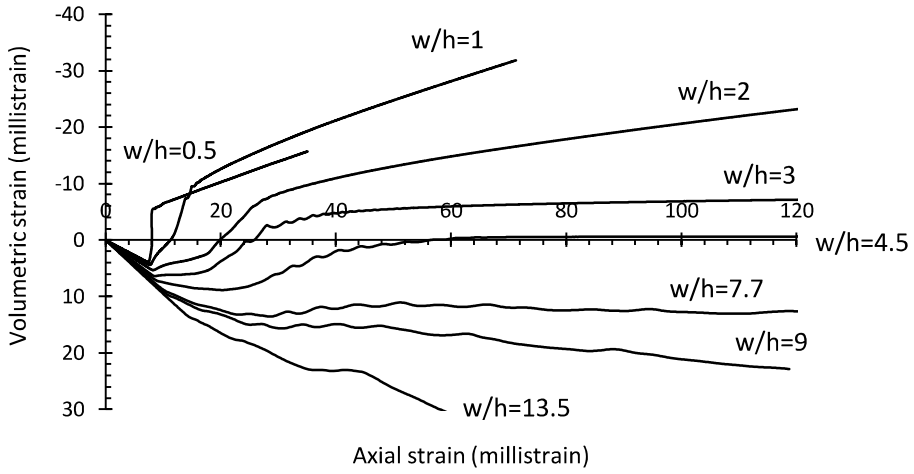

Figure 4.6 Volumetric-axial strain curves of the Singhpur middle coal sample models of various w/h ratio

Figure 4.7 shows the variation in the dilation angle with the w/h ratio and plastic shear strain. The dilation increased from zero to attain its maximum value as the plastic deformation occurred in samples of different w/h ratios. After achieving the peak, the angle gradually decreased and became constant at the later stage. A low w/h ratio resulted in a high peak dilation angle, and the peak value dropped with the increasing w/h ratio of the samples. The rate of decrease in the dilation angle was substantially low with increase in the w/h ratio. Since

the volumetric strain vs axial strain curves of coal samples having w/h ≥ 4.5 did not cross the axial strain axis, the volumetric expansion was equal to or less than the volumetric compaction in these cases. Such samples retained considerable residual strength leading to their controlled failure.

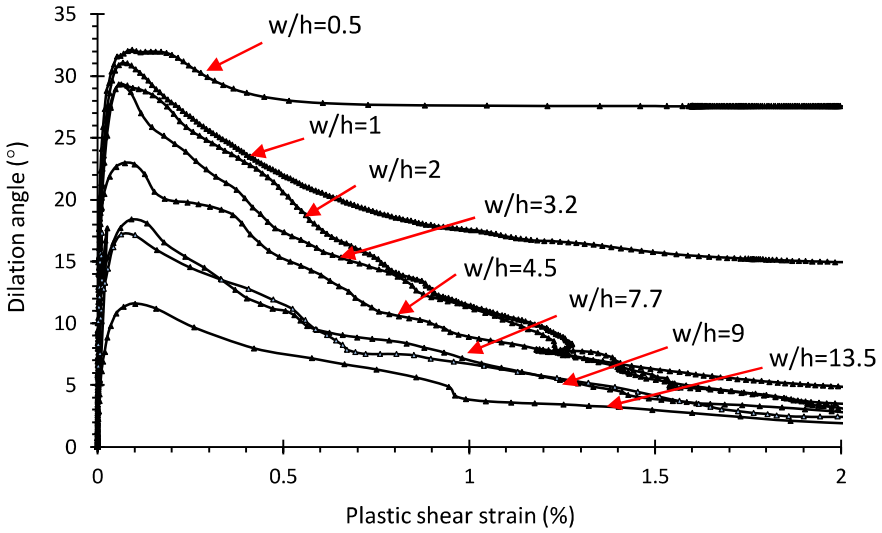

Figure 4.7 Mobilised dilation angle vs plastic shear strain curves of Singhpur middle coal sample models of various w/h ratio

When a sample is axially loaded, the confining stresses are developed throughout its volume due to the confinement provided by the contact surfaces between its ends and the platens, and the shape effect (w/h ratio). Figure 4.8 shows the plot of confining and axial stresses with axial strain in the sample for w/h ratios of 0.5, 4.5, 7.7, and 13.5, exhibiting perfectly brittle, strain softening, perfectly plastic, and strain hardening behaviour, respectively. The peak strength of the sample having w/h of 0.5 was mainly because of the uniaxial compressive strength (UCS), as the confining stress was almost negligible. The strength dropped to zero immediately after

attaining the peak value, resulting in negligible residual strength. In the sample having w/h=4.5, the strength continued to increase beyond the UCS value because of the increasing confining stress, owing to restrictions provided by interfaces and shape effects. After that, continual reduction in confining stress because of increasing width of failure zones at the sample periphery results in softening of the strength. The sample retained considerable residual strength even after failure. The confining stress in the sample of w/h=7.7 grew until the peak strength and remained constant. Consequently, the peak strength of the sample also remains almost constant even after yielding. On the other hand, the strength of the sample having w/h=13.5 continued to increase as the confining stresses generated by the interfaces and shape effects grew almost indefinitely.

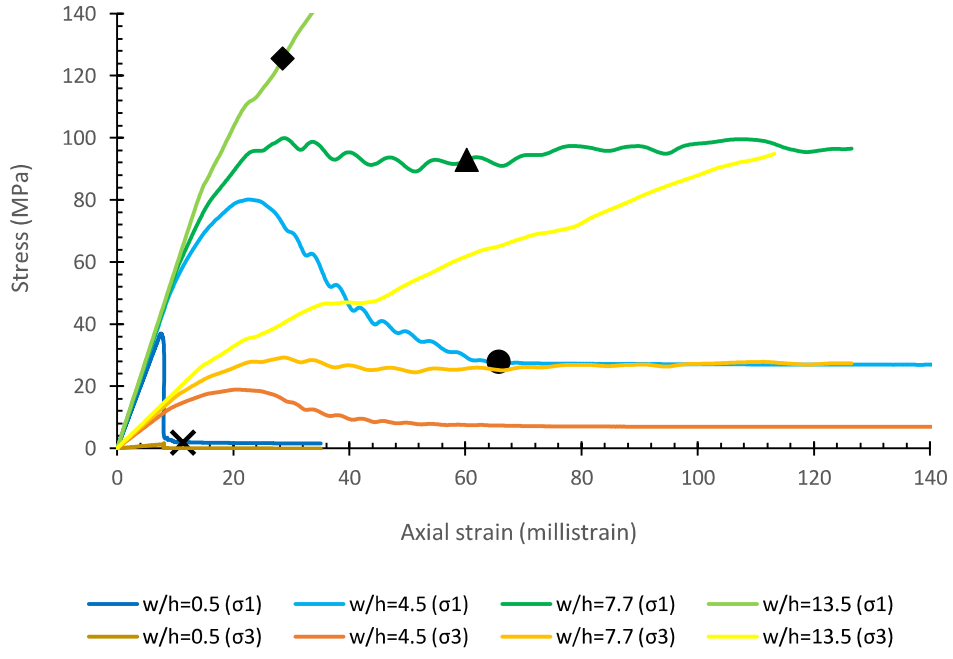

Figure 4.8 Stress-strain profiles of axial and confining stresses for Singhpur middle coal samples of w/h ratio of 0.5, 4.5, 7.7, and 13.5, depicting different post-failure behaviour: brittle, softening, ductile, and continuous strain-hardening

Figure 4.9 shows the shear slip and displacement along with the interface and type of failure at the specimen top-end for w/h of 0.5, 4.5, 7.7, and 13.5 at the loading stage highlighted by the cross, circle, triangle, and rhombus markers in Figure 4.8. The actual shear slip of the interface is depicted by the 'Slip Now' state, while the 'shear slip in past' occurred during the first few steps of the solution due to transient stresses. The top-end surface of the coal sample, having a w/h ratio of 0.5, did not show any state of failure. The slippage of the interface occurred asymmetrically on one side, resulting in a substantial shear displacement of the interface on the affected side. This failure at the top end was due to axial splitting or hour-glass failure of the sample.

On the other hand, three distinct zones: core zone, transition zone, and rib zone, can easily be identified by blue, green, and red contours of interface shear displacement for the samples having w/h ratios of 4.5, 7.7, and 13.5. The core zone has higher confining stress as it is confined by broken or yielded material, and the rib zone has very little or no confining stress as it is exposed to the traction-free surface. The transition zone shows a wide range of confining stress, increasing from the rib zone towards the core zone. The top-end surface of the sample having a w/h ratio of 4.5 failed till the core, but the interface slip did not reach the core. Hence, a constant confining stress was maintained due to the confinement provided by the failed material and interface effect resulting in a continued and substantial residual strength.

For the sample having w/h of 7.7, a part of the core was elastic, and no interface slip was observed above the core. Hence, it maintained a significantly high residual strength owing to the interface effect. For w/h of 13.5, only the edge of the top-end surface yielded in shear because of the limited shear slip at the edge of the interface. The sample showed strain-hardening characteristics in this case. These observations provide a further extension of the work reported by Prassetyo (2011), Lu et al. (2008) and Morsy (2003).

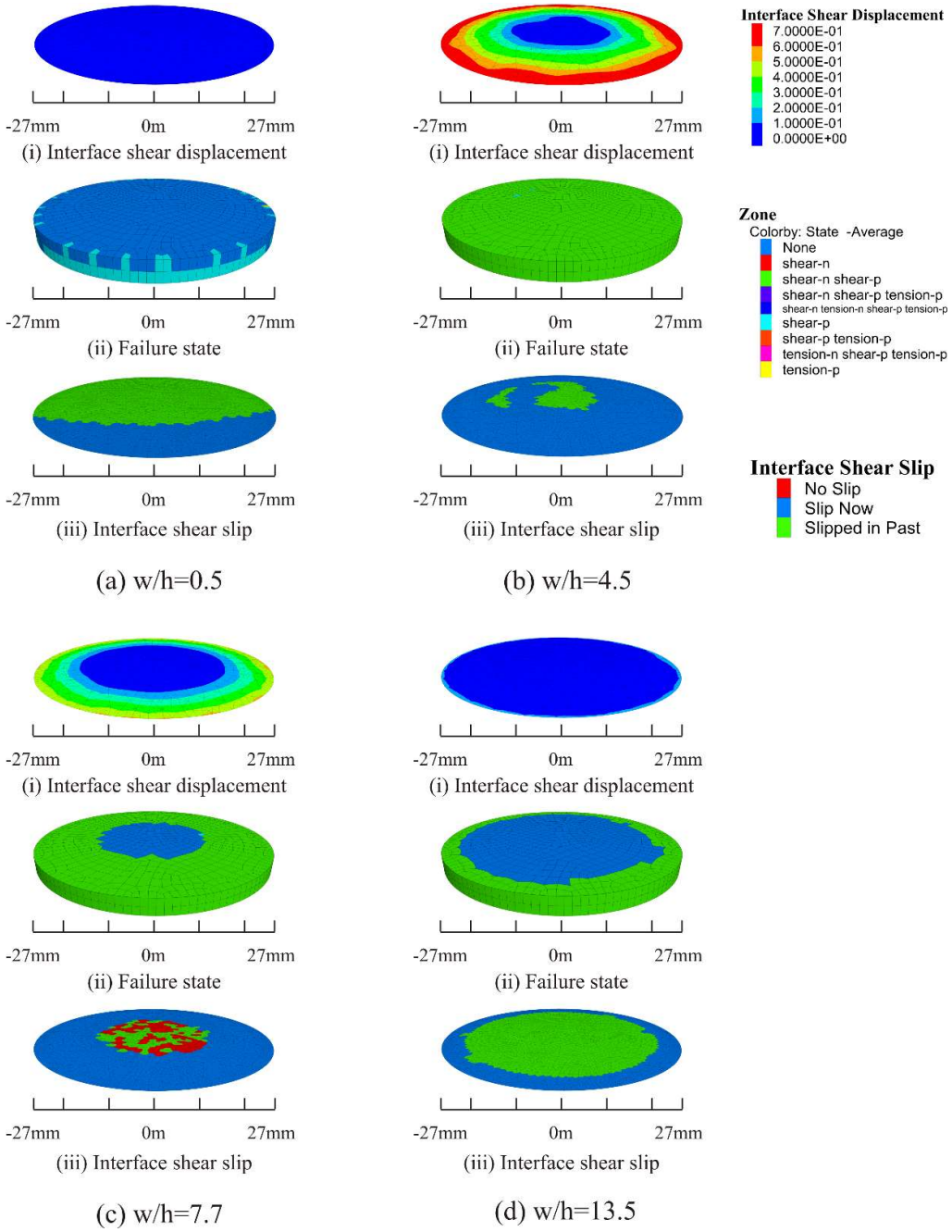

Figure 4.9 Slip along the interface due to shearing, failure state of the top end-surface of the coal sample, and shear displacement of the interface for samples having w/h ratio of (a) 0.5, (b) 4.5, (c) 7.7, and (d) 13.5 at the loading stage highlighted by the cross, circle, triangle, and rhombus markers in Figure 4.8

Figure 4.10 illustrates the volumetric strain of the samples versus the differential stress. The point where the characteristic curve intersects the differential stress axis marks the state when the increase in volumetric strain due to the propagation and coalescence of existing cracks and the formation of new cracks is equal to the decrease in the volumetric strain due to the compaction of pores and existing cracks in the samples. It is noted that the curves for samples having a w/h ratio greater than 4.5 did not cross the stress axis owing to greater confinement as the combined effect of the interface and the shape effects restricted the volumetric expansion of the samples. An opposite trend was observed for samples having w/h less than 4.5. These trends confirmed that samples having w/h > 4.5 could hardly undergo substantial dilation and sudden failure. These observations of the modelled samples are in close agreement with the laboratory test results and the rock mechanics theories (Zhao and Cai, 2010).

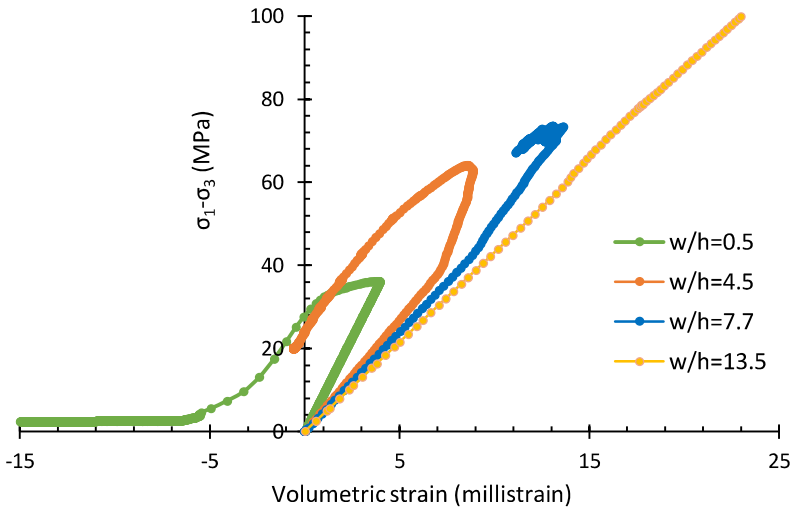

Figure 4.10 Model observed volumetric strain vs differential stress, illustrating relative volumetric changes due to new cracks formation or propagation of existing ones and compaction of pores or existing cracks

4.5 Statistical Models for Post-Peak Strength Parameters

Table AIII.1 presents the final drop rate and residual values of the calibrated numerical models with zone sizes of 0.5, 1, and 2 mm for samples of various w/h ratios from six Indian coal seams. The data pf drop rates and the residual values of 126 calibrated models indicated that the drop rate in friction angle is constant for almost all the cases. Accordingly, a constant drop rate of either 300 or 500°/plastic shear strain was decided for the friction angle of the coal. Further analysis suggested that the cohesion drop rate, residual cohesion and residual friction angle are non-linearly correlated with UCS, friction angle ($\boldsymbol{\phi}$), elastic modulus (E) and the zone size (zs). Equations 4.1-4.4 show the statistical models for estimating the drop rates and residual values of the MC strength parameters to characterise the strain-softening behaviour of the coal. These relations are valid for zone sizes ranging from 0.5-2 mm.

The constant value of the drop rate as obtained in this study is consistent with Mohan et al. (2011). They suggested a constant drop rate of 500 °/plastic shear strain for the friction angle, based on the back analysis of failed and stable cases of pillars in Indian coal mines.

$$c_{drop} = 635.26\frac{{\sigma_c}^{0.85} \cdot (w/h)^{0.07} \cdot E^{0.89} \cdot zs^{0.71}}{\phi^{1.78}}, \quad R^2 = 0.78 \tag{4.1}$$

$$c_{res.} = \begin{cases} 0 \quad \forall \ w/h < 2 \\ 6.56 \cdot \ln\left(\frac{w}{h}\right) + 0.24 \quad \forall \ w/h \geq 2, \end{cases} \quad R^2 = 0.68 \tag{4.2}$$

$$\phi_{drop} = 300 \ or \ 500 \tag{4.3}$$

$$\phi_{\text{res.}} = 594.44\frac{(\text{w/h})^{0.09}}{\phi^{0.64}}, \quad R^2 = 0.45 \tag{4.4}$$

where c_{drop}, ϕ_{drop}, $c_{res.}$, and $\phi_{\text{res.}}$ are in MPa/plastic shear strain, °/plastic shear strain, percentage of peak cohesion (c) and friction angle (ϕ), respectively. σ_c (MPa) and E (GPa) are

the compressive strength and elastic modulus of the rocks, respectively. 'w' and 'h' are the effective width and height of the sample.

Figure 4.11 compares the outcome of the statistical model and the numerical modelling results for the 126 calibrated models (Table AIII.1). The projections of the statistical model are in close agreement with the numerical modelling results.

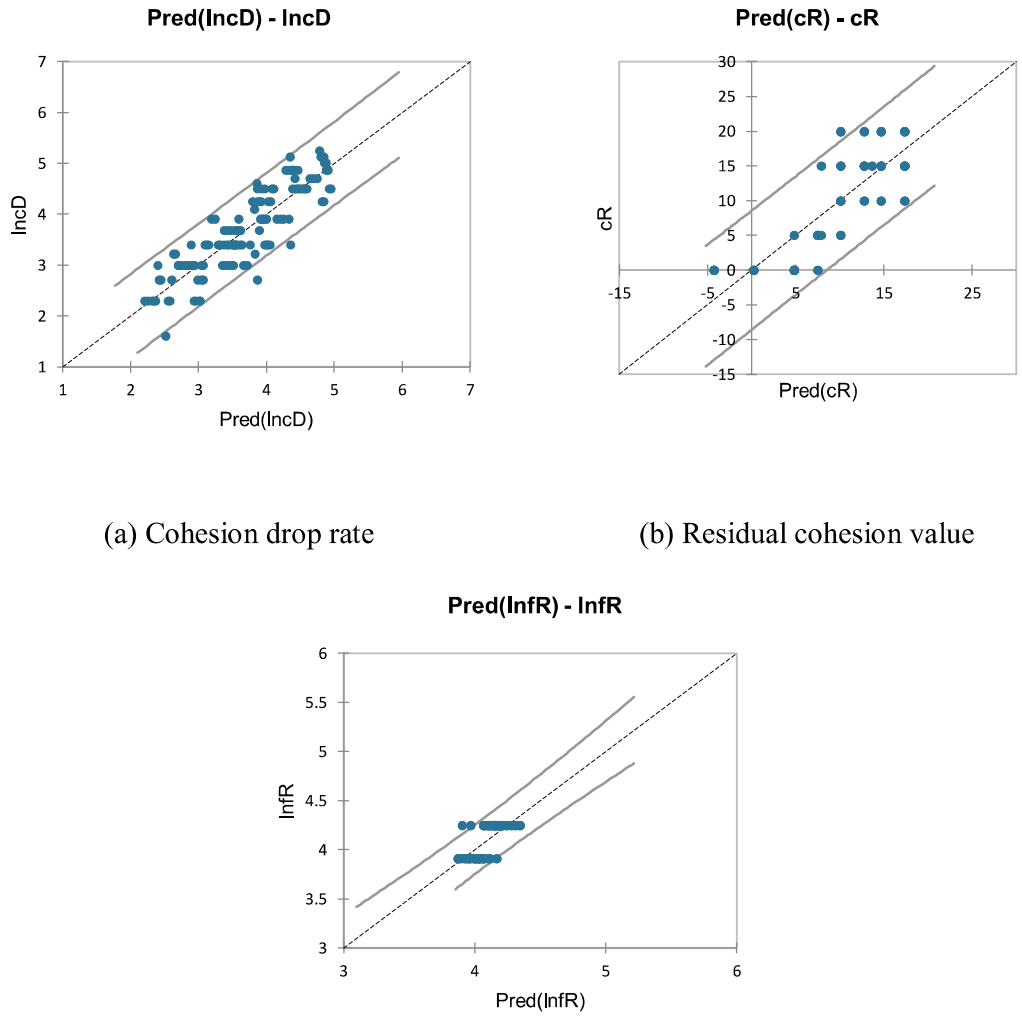

(a) Cohesion drop rate

(b) Residual cohesion value

(c) Residual friction angle value

Figure 4.11 Comparison between the statistically predicted values and the numerical model for (a) Cohesion drop, c_{drop} (b) Residual cohesion, c_{res} and (c) residual friction $\boldsymbol{\phi_{res.}}$ on a logarithmic scale

4.6 Model Validation

The validity of the developed model was verified using the results of triaxial compression tests reported by Medhurst (1996) on 61 and 146 mm diameter coal samples. He conducted a series of triaxial tests on coal samples of 61, 101, 146, and 300 mm in diameter to investigate the scale effect on the mechanical behaviour of coal and concluded that the failure mechanism changed from axial splitting to shear failure depending upon the magnitude of confining stress.

The deformation modulus of 61mm and 146 mm diameter samples were 4 GPa and 1.9 GPa, respectively. The Poisson's ratio of 0.25 was assumed. The model geometry and boundary conditions were similar to the uniaxial test models (Section 3.9, Chapter 3), except that the grid forces equivalent to the confining stresses applied during laboratory tests were initialised to simulate the triaxial compression tests. The post-peak softening parameters were estimated using the developed statistical model (Equations 4.1 - 4.4). The peak and strain-softening parameters for the sample diameter of 61mm and 46mm are shown in Figure 4.12.

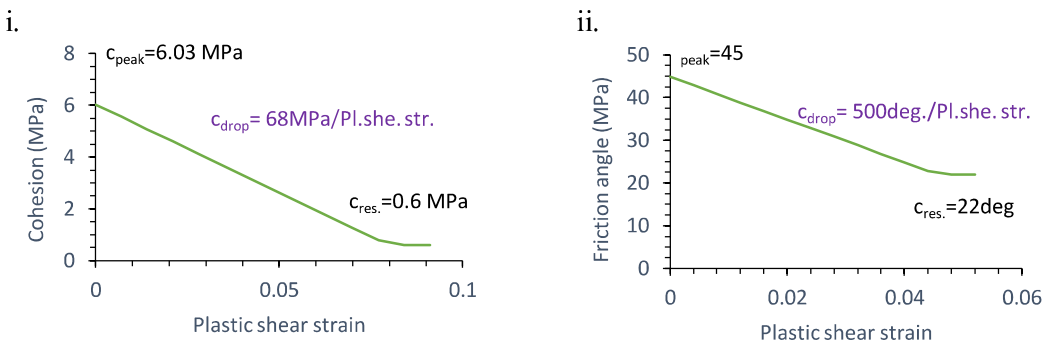

(a) Diameter = 61 mm

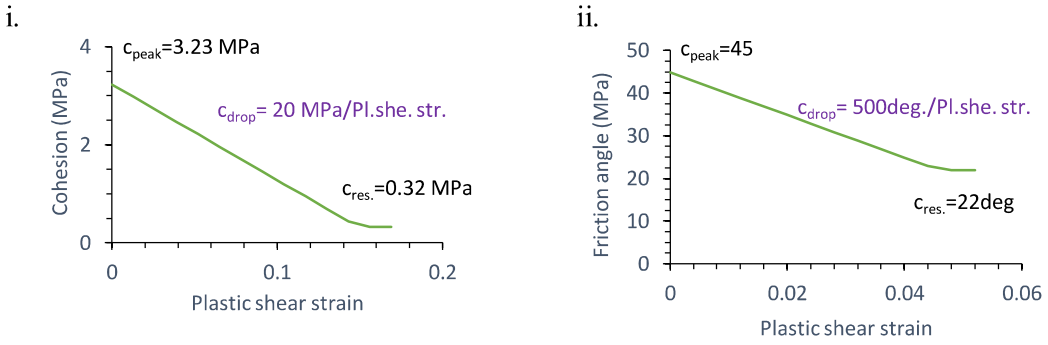

(b) Diameter = 146 mm

Figure 4.12 Drop rate, peak, and residual values of (i) cohesion and (ii) friction angle of the coal samples of (a) 61 and (b) 146 mm diameter

Figures 4.13 and 4.14 compare the mechanical and dilation behaviour obtained in the numerical model and the laboratory test for different diameters of the coal samples at low to high confining stresses. Medhurst (1996) repeated the triaxial test on several samples from the same coal seam. The legends of the charts show the code of samples from the same coal seam. The model results are in close agreement with the laboratory test results, given the existing variability in the test results. They also capture the smooth trend of decreasing dilation with increasing confining stress in the coal sample. The peak and residual strengths gradually increased with the confining stress, in line with the test results.

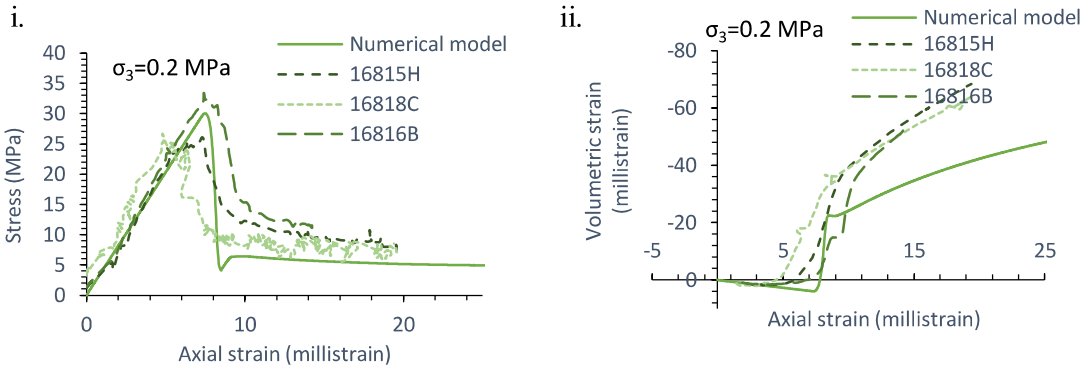

(a) Confining stress = 0.2 MPa

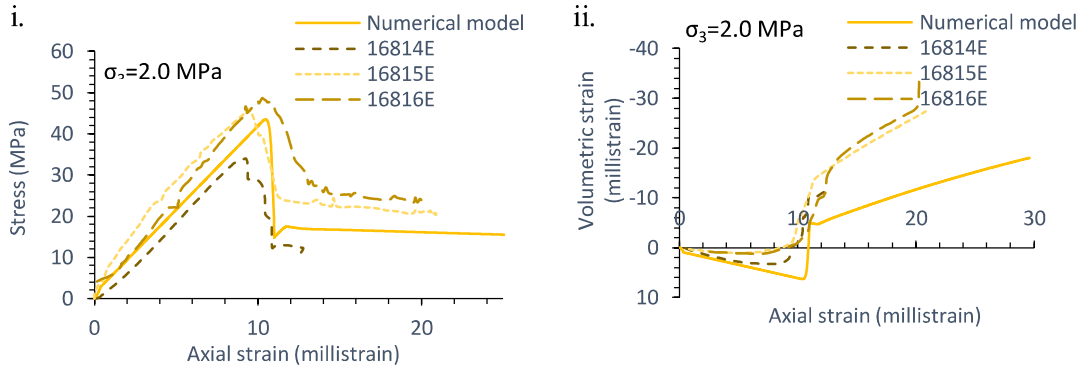

(b) Confining stress = 2 MPa

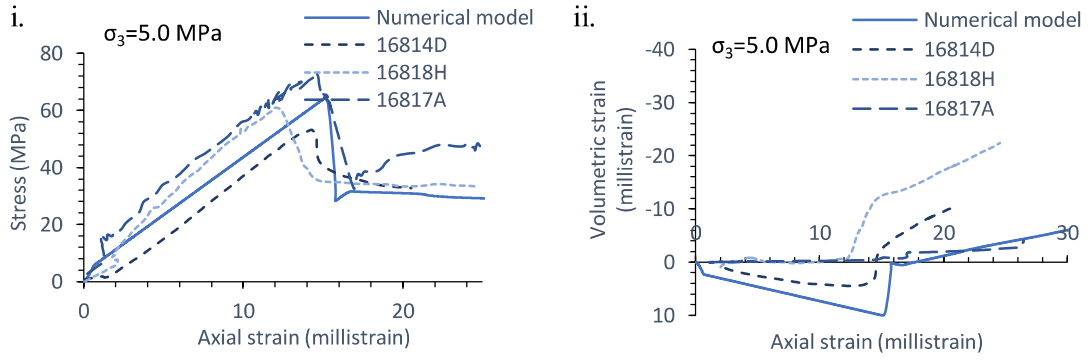

(c) Confining stress = 5 MPa

Figure 4.13 The comparative plot of the laboratory tests results (Medhurst, 1996) and numerical model of (i) axial stress – strain and (ii) volumetric – axial strain for confining stress of (a) 0.2, (b) 2.0, and (c) 5.0 MPa for 61 mm diameter coal samples

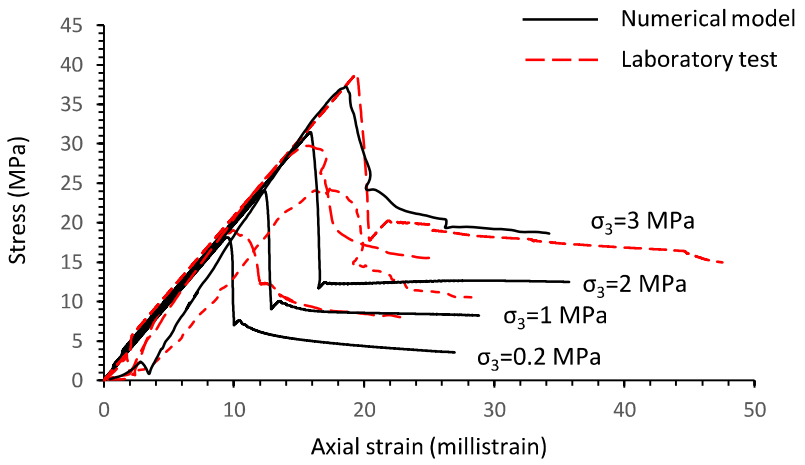

(a)

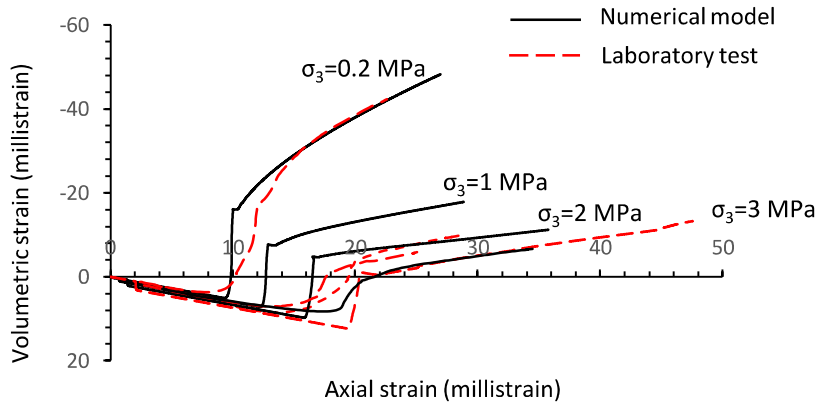

(b)

Figure 4.14 Laboratory tests results (Medhurst, 1996) vs the numerical model results of axial stress-strain (a) and volumetric - axial strain (b) at confining stress of 0.2, 1.0, 2.0, and 3.0MPa for 146 mm diameter coal samples

Figure 4.15 illustrates the failure patterns observed in the numerical models and the laboratory tests for 61 mm diameter coal samples subjected to confining stress of 0.2, 2.0, and 5.0 MPa. Axial splitting of the sample was observed at confining stress of 0.2 MPa, which is captured by the model in the shape of an hour-glass failure. The observed failure pattern corroborates well with Bai et al.'s (2014, 2017) observations. Further, the shear failure mechanism was observed in the modelled samples subjected to confining stresses of 2.0 and 5.0MPa, which corroborates well with the test results. The validity of the softening model is further reinforced in Chapter 5, where the failed and stable cases of pillars representing the Indian geo-mining conditions have been simulated.

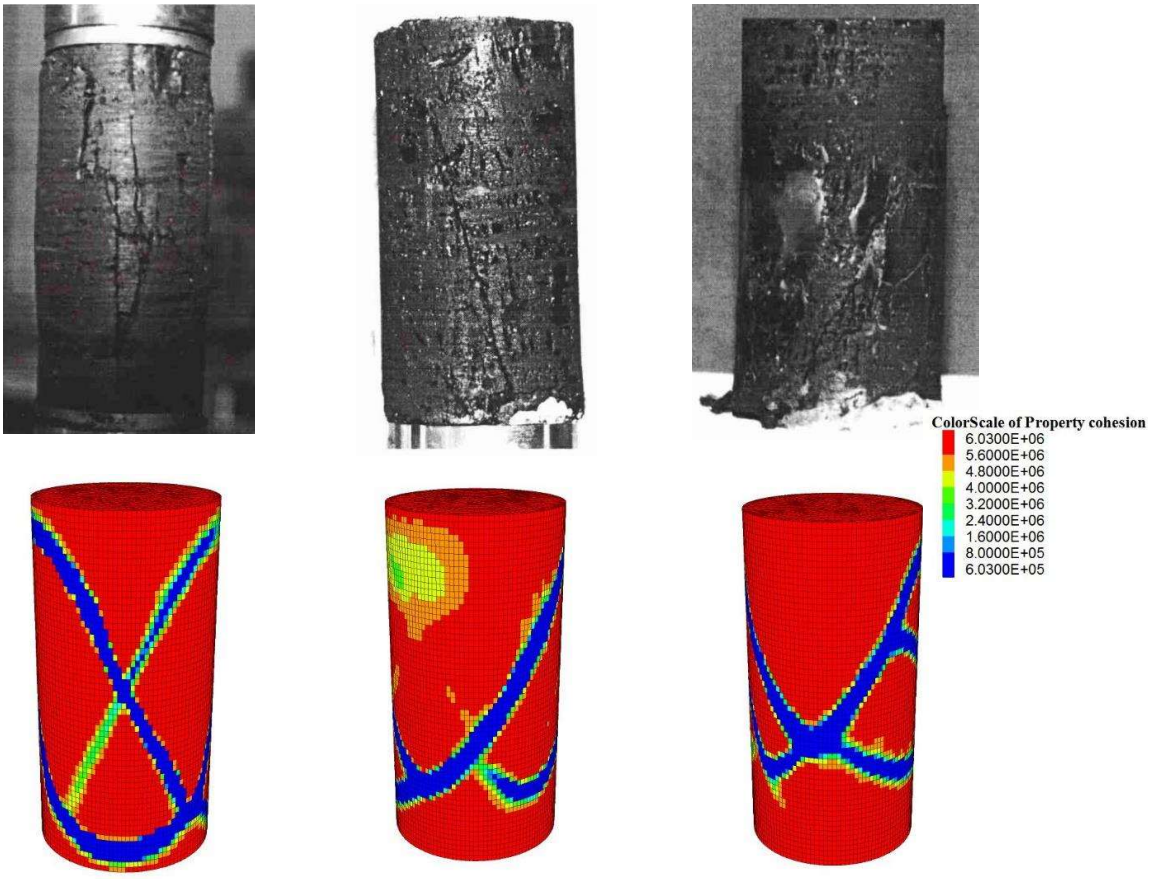

(a) (b) (c)

Figure 4.15 Failure mechanism observed in the laboratory tests (top) (Medhurst, 1996) and numerical models (bottom) for confining stresses of (a) 0.2, (b) 2.0, and (c) 5.0 MPa

4.7 Summary

A numerical simulation study was carried out to develop a standard approach for estimating the post-peak strength parameters for different w/h ratios of coal pillars based on the laboratory test data of coal samples from different coal seams in India. It involved calibrating the model observed stress-strain curve with the laboratory observed profiles. It was assumed that both the cohesive strength and the friction angle degraded with the evolving plastic damage in the coal material. The plastic damage in the continuum media was quantified using plastic shear strain, and confinement provided by the contact surfaces at the specimen ends was simulated using interface elements available in FLAC^{3D}. The volumetric expansion in the coal following the plastic damage was simulated using the W-D dilation angle model (Section 3.4.2). The models were run with zone sizes of 0.5, 1, and 2 mm to study the effect of the zone size on the post-peak strength parameters. The data generated from the 126 calibrated models were used to develop the statistical models for estimating the post-peak strength parameters.

The outcomes of calibrated models showed that post-peak strength parameters varied with the zone size, w/h ratio, strength and deformation properties. The variation in post-peak strength was primarily governed by the rate of drop in cohesion and its residual value. The cohesion drop rate increased with increasing w/h ratio and zone size. The residual cohesion for w/h $\leq$2 was zero. On the other hand, a drop rate of either 300 or 500°/plastic shear strain in the friction angle was suggested for a conservative strength estimate. The residual friction of 50- 70% of its peak value was adequate for different coal samples.

The calibrated models were used to study the post-failure dilatancy behaviour and the effect of the interface on the mechanical behaviour of the samples. The observations showed that the dilation angle decreases with the increase in the w/h ratio and the plastic shear strain. An in-depth analysis of confinement with the axial strain in the modelled samples showed that the sample with a low w/h ratio had negligible confining stress, whereas the sample with a high

w/h ratio had more significant confining stress. The confining stress in the latter case continued to increase for axial strain beyond the peak strength value. On closer scrutiny, it was found that the confinement provided by the interface in conjunction with the w/h ratio significantly influenced the post-peak strength of the samples.

The coal sample with an adequate w/h ratio was able to retain substantial residual strength, although it had failed up to the core because of the confinement provided by the residual strength of failed elements and the contact surfaces between the platens and the specimen ends. The differential stress versus volumetric strain curves showed that the likelihood of sudden failure was low beyond a specific w/h ratio, which was 4.5 in the case of the Singhpur middle coal seam. The coal samples with a higher w/h ratio had a controlled failure. The data points generated from the calibrated models were used to develop a set of statistical models to estimate the post-peak strength parameters for a given set of geometric, strength and deformability properties of coal. The validation of the statistical model using the triaxial test results reported by Medhurst (1996) showed a very close agreement.